LYMPHOID NEOPLASIA

Mechanisms of PD-L1/PD-1–mediated CD8 T-cell dysfunction in the context of aging-related immune defects in the Eμ-TCL1 CLL mouse model

Fabienne McClanahan,[1,2] John C. Riches,[1] Shaun Miller,[1] William P. Day,[1] Eleni Kotsiou,[1] Donna Neuberg,[3] Carlo M. Croce,[4] Melania Capasso,[5] and John G. Gribben[1]

[1]Centre for Haemato-Oncology, Barts Cancer Institute, Queen Mary University of London, London, United Kingdom; [2]Department of Molecular Genetics, German Cancer Research Center, Heidelberg, Germany; [3]Department of Biostatistics and Computational Biology, Dana-Farber Cancer Institute, Boston, MA; [4]Department of Molecular Virology, Immunology, and Medical Genetics, The Ohio State University, Columbus, OH; and [5]Centre for Cancer and Inflammation, Barts Cancer Institute, Queen Mary University of London, London, United Kingdom

Key Points

- PD-L1/PD-1–mediated CD8 T-cell dysfunction develops with CLL in different organs, and similarities to aging-related immune defects exist.
- PD-1$^+$ normal T cells have markedly different effector functions than PD-1$^+$ CLL T cells.

T-cell defects, immune suppression, and poor antitumor immune responses are hallmarks of chronic lymphocytic leukemia (CLL), and PD-1/PD-L1 inhibitory signaling has emerged as a major immunosuppressive mechanism. However, the effect of different microenvironments and the confounding influence of aging are poorly understood. The current study uses the Eμ-TCL1 mouse model, which replicates human T-cell defects, as a preclinical platform to longitudinally examine patterns of T-cell dysfunction alongside developing CLL and in different microenvironments, with a focus on PD-1/PD-L1 interactions. The development of CLL was significantly associated with changes in T-cell phenotype across all organs and function. Although partly mirrored in aging wild-type mice, CLL-specific T-cell changes were identified. Murine CLL cells highly expressed PD-L1 and PD-L2 in all organs, with high PD-L1 expression in the spleen. CD3$^+$CD8$^+$ T cells from leukemic and aging healthy mice highly expressed PD-1, identifying aging as a confounder, but adoptive transfer experiments demonstrated CLL-specific PD-1 induction. Direct comparisons of PD-1 expression and function between aging CLL mice and controls identified PD-1$^+$ T cells in CLL as a heterogeneous population with variable effector function. This is highly relevant for therapeutic targeting of CD8$^+$ T cells, showing the potential of reprogramming and selective subset expansion to restore antitumor immunity. (*Blood*. 2015;126(2):212-221)

Introduction

Chronic lymphocytic leukemia (CLL) is characterized by profound immune defects, leading to severe infectious complications and lack of adequate antitumor immune responses. These deficiencies are caused by complex, bidirectional interactions between malignant cells and components of the tumor microenvironment.[1] In particular, T cells are numerically, phenotypically, and functionally highly abnormal, with only limited abilities to exert antitumor immune responses.[2] Our previous work demonstrated that T cells from CLL patients show highly impaired immune synapse formation, cytotoxic function, and T-cell adhesion/migration resulting from ineffective regulation of actin-cytoskeleton remodeling.[3-6] This is mediated by aberrant expression of several inhibitory receptors on CLL cells, prominently PD-L1 (CD274).[7] The corresponding binding partner of PD-L1, PD-1 (CD279), is a major inhibitory receptor associated with T-cell exhaustion, a state of functional hyporesponsiveness caused by chronic infections.[8-11] Binding of PD-1 to PD-L1 and PD-L2 results in repressed T-cell receptor signaling, proliferation, and motility.[12-15] However, recent evidence suggests that this is neither an irreversible, terminal differentiation state nor an unresponsive T-cell state; instead, T cells with an exhaustion phenotype represent a heterogeneous population, in which subsets are, despite PD-1 expression, able to maintain and exert certain effector functions.[16,17]

CD8$^+$ T cells from CLL patients exhibit some features of exhaustion such as increased PD-1 expression, but conflicting data exist on its functional impact: although we have described impaired T-cell proliferation and cytotoxicity with maintained interferon-γ (IFN-γ)/tumor necrosis factor-α production,[4] increased PD-1 expression on proliferating compared with nonproliferating T cells along with impaired IFN-γ/interleukin-4 (IL-4) production has been reported by others.[18] Interestingly, this was also observed after stimulation of T cells from healthy controls, albeit at a lower degree, suggesting a somewhat constrained physiological reaction in CLL T cells. PD-1$^+$ T cells in CLL therefore appear to be a highly heterogeneous population, in which certain effector functions might be maintained despite PD-1 expression. However, the functional characteristics of these populations and how distinct states of dysfunction develop in the context of advancing CLL remain poorly understood. This is further complicated by the finding that PD-1 expression plays an important role in T-cell homeostasis in

Submitted February 4, 2015; accepted May 12, 2015. Prepublished online as *Blood* First Edition paper, May 15, 2015; DOI 10.1182/blood-2015-02-626754.

The online version of this article contains a data supplement.

There is an Inside *Blood* Commentary on this article in this issue.

The publication costs of this article were defrayed in part by page charge payment. Therefore, and solely to indicate this fact, this article is hereby marked "advertisement" in accordance with 18 USC section 1734.

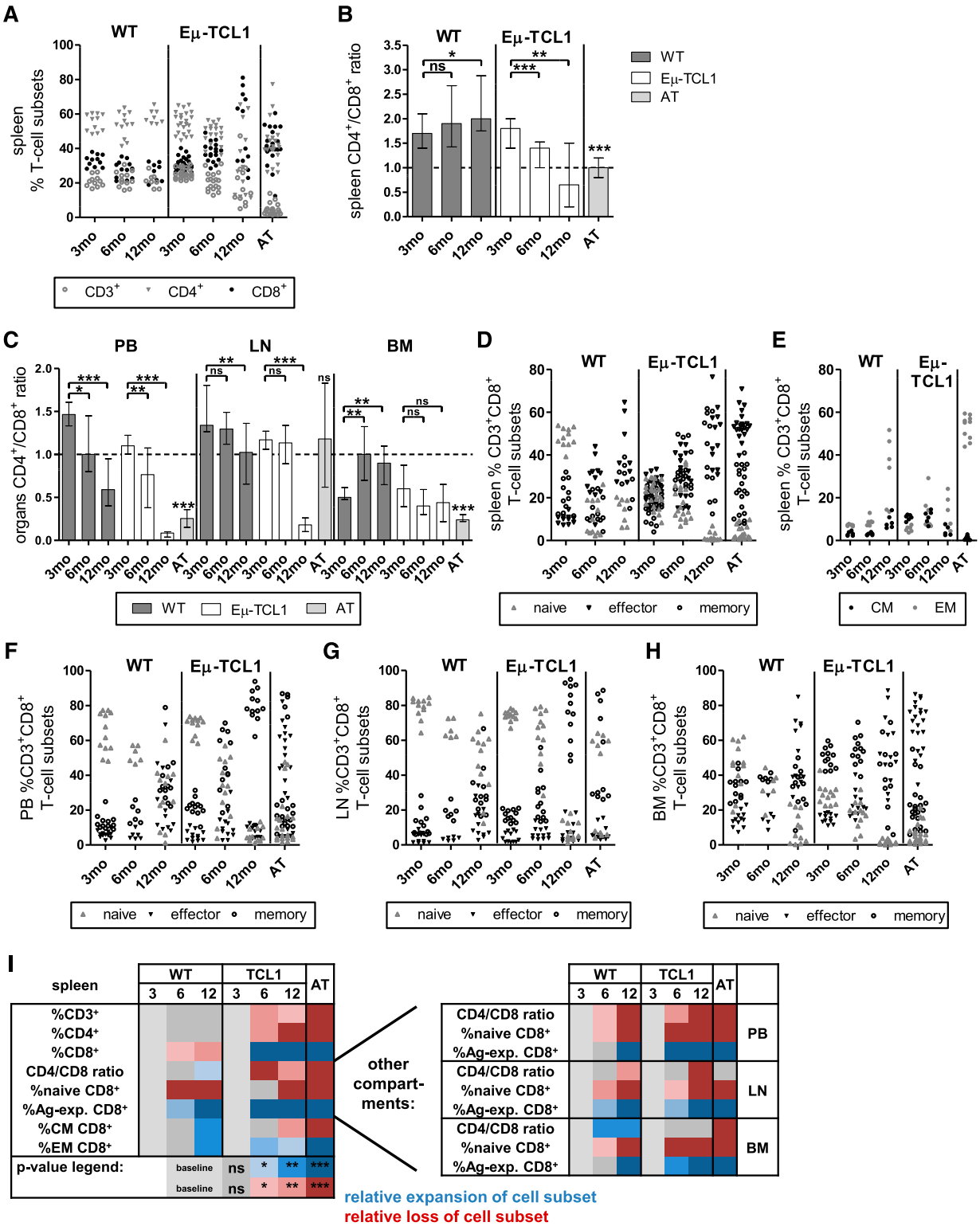

Figure 1. Longitudinal changes of T-cell subsets in PB and CLL-affected organs in aging Eμ-TCL1 and WT mice and after AT. At least 2 cohorts of 3-, 6, and 12-month (mo)-old Eμ-TCL1, WT, and AT mice containing ≥5 mice each were euthanized and PB, and single-cell suspensions of CLL-affected organs were stained for CD3, 4, 8, 62L, 44, and CCR7 (spleen only) and assessed in relation to CLL load (supplemental Figure 1). Dead cells were excluded by 4,6 diamidino-2-phenylindole. Groups were compared with 3-month-old mice. Mann-Whitney test was used for nonnormally distributed data and unpaired *t* test for normally distributed data, as determined by Shapiro-Wilk normality test. (A) Longitudinal changes of percentages of $CD3^+$, $CD3^+CD4^+$, and $CD3^+CD8^+$ cells in spleens, leading to (B) changes in $CD4^+/CD8^+$ ratios in spleen, which were recapitulated in (C) PB, LNs, and BM. (D) Longitudinal changes of percentages of spleen $CD44^-CD62L^+$ naive, $CD44^+CD62L^+$ memory, $CD44^+CD62L^-$ effector, and (E) $CD62L^+CCR7^+$ central memory (CM) and $CD62L^-CCR7^-$ EM $CD3^+CD8^+$ cells. Longitudinal changes of percentages of naive, memory, and effector $CD3^+CD8^+$ cells in (F) PB, (G) LNs, and (H) BM (EM and CM cells were not assessed in these compartments/organs). All graphs depict median ± interquartile range and combine data from at all cohorts of mice at each age group. (I) Heat map summary of *P* values describing statistical differences in T-cell subsets in spleen identifying CLL-specific T-cell subset phenotype vs aging-related patterns. Groups were compared with 3-month-old mice. Blue, expansion; red, loss of cell subsets; ns = nonsignificant. $^*P < .05$, $^{**}P < .001$, $^{***}P < .0001$.

healthy older humans.[19] This needs to be taken into account when interpreting PD-1 and immune function in CLL because it is predominantly a disease of the elderly. Moreover, the majority of studies on PD-L1/PD-1 in CLL have been conducted in peripheral blood (PB). For CLL cells, characteristic tissue- and compartment-specific gene signatures,[20,21] CD38 expression patterns,[22,23] proliferation,[24] and apoptotic regulation mechanisms[25,26] are now well-recognized. The importance of different microenvironments on T-cell defects, their association with PD-1 expression, and their contribution to the interactions between PD-L1 expressing CLL and PD-1 expressing T cells are in contrast still poorly understood.

The majority of these questions can only be partly addressed in human CLL. Because development of CLL in transgenic Eμ-TCL1 mice[27] is associated with global T-cell defects very similar to those observed in human patients,[28,29] this mouse model offers a powerful preclinical platform to investigate T-cell–directed questions in the context of aggressive CLL. The aims of the current study were therefore to use the Eμ-TCL1 model to examine the longitudinal development of T-cell dysfunction in the context of advancing CLL; to identify the impact of different microenvironments on T-cell defects and PD-L1, PD-L2, and PD-1 expression; and to elaborate the functional impact of PD-1 expression on T-cell effector function.

Methods and materials

Mice and in vivo procedures

All animal work was carried out following local ethical regulations. Disease status was monitored by physical examination and hematology testing. Aging Eμ-TCL1 mice were euthanized at 3, 6, and 12 months of age or when fully leukemic (for initial characterization of PD-L1, see Figure 3A-C). Age-matched wild-type (WT) littermates and WT mice from commercial suppliers served as controls. In adoptive transfer (AT) experiments, young CLL-free mice received 4×10^7 frozen splenocytes from leukemic Eμ-TCL1 donors (%$CD19^+CD5^+$ CLL cells routinely confirmed >95%) or an equal dose of WT spleen B cells by IV injection. AT and leukemic Eμ-TCL1 mice were euthanized once they exhibited white blood cell counts >100 white blood cells/hpf (×40 objective), >90% lymphocytes $CD19^+CD5^+$ CLL cells, and/or spleen size >3 cm compressing other organs.

Tissue preparation

PB was collected in EDTA-coated Eppendorf tubes by cardiac puncture. Spleen single-cell suspensions were prepared using an automated tissue dissociator (Miltenyi, UK) per manufacturer's recommendations. Lymph nodes (LNs) were dissociated manually. Femurs were flushed with fluorescence-activated cell sorter buffer. Although the peritoneal cavity is an area of interest in mice, this was not examined here because we focused on compartments of particular relevance in human disease.

Immunophenotyping by multicolor flow cytometry

Surface staining was performed in phosphate-buffered saline/2% fetal calf serum for 30 minutes at 4°C following standard procedures using anti-CD5, CD19, CD3, CD4, CD8, CD44, CD62L, PD-L1/2, PD-1, KLRG-1, LAG-3, and 2B4 antibodies (all from eBioscience or Biolegend, UK). CCR7 staining was performed at 37°C for 20 minutes. Fluorescence-minus-one (FMO), internal negative, and/or isotype controls were always included. Gating strategies and definition of populations are summarized in supplemental Figure 1A-B on the *Blood* Web site. Samples were acquired on a BD LSRII Fortessa (BD, UK). Flow cytometry standard files were analyzed by FlowJo software, version 7. Absolute numbers (ANs) in PB, LN, and bone marrow (BM) cell suspensions were enumerated using CountBright counting beads (Molecular Probes, UK). ANs in the spleen were enumerated by multiplying the percentages of populations of interest with total cell numbers of whole-organ, single-cell suspensions counted by a ViCell hemocytometer (Beckman-Coulter, UK), as reported by others.[30]

Functional flow cytometry assays

Flow cytometry–based functional assays were performed on fresh T cells ± phorbol-12-myristrate-13-acetate (40.5 μM)/ionomycin (670 μM) mitogenic stimulation for 6 hours in the presence of brefeldin A (5.3 mM)/monensin (1 mM, eBioscience, UK) for the last 5 hours. Effector-cell activity was assessed by CD107a surface expression[31] and intracellular Granzyme B (GrB), IL-2, IL-4, and IFN-γ levels in stimulated $CD4^+$ and $CD8^+$ cells (supplemental Figure 1C). Intranuclear ki-67 was determined on unstimulated $CD8^+$ cells. To account for differences and dynamic changes of percentages of $CD44^+$ cells between WT/Eμ-TCL1 mice and age groups, effector-cell function was described as a ratio of $CD44^+CD107a^+/GrB^+/cytokine^+/ki\text{-}67^+$ cells over $CD44^+CD107a^-/GrB^-/cytokine^-/ki\text{-}67^-$ cells among $CD3^+CD8^+$ cells (supplemental Figure 1D). Increased ratios were interpreted as enrichment and decreased ratio as loss of those effector cells among $CD44^+$ populations, which is a more biologically accurate estimation of effector function than mere comparisons of %positive cells within overall different $CD44^+$ subsets.

In vivo proliferation

Mice were injected intraperitoneally with 100 μg/g body weight 5-ethynyl-2′-deoxyuridine (EdU, Life Technologies, UK) 20 hours before euthanasia. Splenocytes were prepared for EdU detection by AlexaFluor488 dye following the manufacturer's instructions and stained for CD5, CD19, CD8, and PD-1. Analysis was performed on single mononuclear cells, and proliferating cells were identified as $AlexaFluor488^+$ populations based on negative internal controls without AlexaFluor488 in the EdU reaction cocktail.

Immune synapse formation assays

CLL and B cells were obtained from frozen splenocytes by magnetic isolation using murine CD19 microbeads (Miltenyi). The column effluent representing the $CD19^-$ fraction was purified by negative selection (murine pan-T-cell isolation kit, Miltenyi). $CD3^+CD8^+PD\text{-}1^{high}$ and $PD\text{-}1^{low}$ populations were isolated by flow sorting on a BD Aria II. Synapse assays and confocal microscopy were performed as previously described.[3] The AxioVision outline tool (Zeiss) was used to mark each synapse between T and B cells, and all available interactions were scored in each condition. The synapse area was reported as the area of T-cell F-actin immune synapses (μm^2) value.

Statistical considerations

To account for batch/litter effects, phenotyping experiments were conducted at least twice with a minimum of 5 matched mice/group. Functional experiments and ANs were determined once in ≥6 mice/group (aging mice) and twice in AT mice (≥4 mice/group). Because mice showed no evidence for unexpected litter effects ($P > .05$ for each), experimental groups were analyzed and depicted together. Data sets were subjected to normality testing using the Shapiro-Wilk normality test. Differences between data sets modeled by Gaussian distribution were analyzed by unpaired *t* test; otherwise, the 2-sided Mann Whitney *U* test was used. Statistical dependence between 2 quantitative variables was assessed by Spearman's rank correlation coefficient modeling. *P* values $< .05$ were considered statistically significant. Analyses were conducted using Prism Version 5 software (GraphPad). *P* values were visualized with the help of heat map summaries in selected experiments, with shades of blue/red applied to express different significance levels (ie, $P < .05$, $P < .001$, $P < .0001$). Values in figures are reported as median and interquartile range, unless indicated otherwise.

Results

Developing CLL is associated with specific T-cell subsets changes in spleen, PB, BM, and LNs

To determine CLL load/development, PB and single-cell suspensions from BM, LNs, and spleens of 3-, 6-, and 12-month-old Eμ-TCL1,

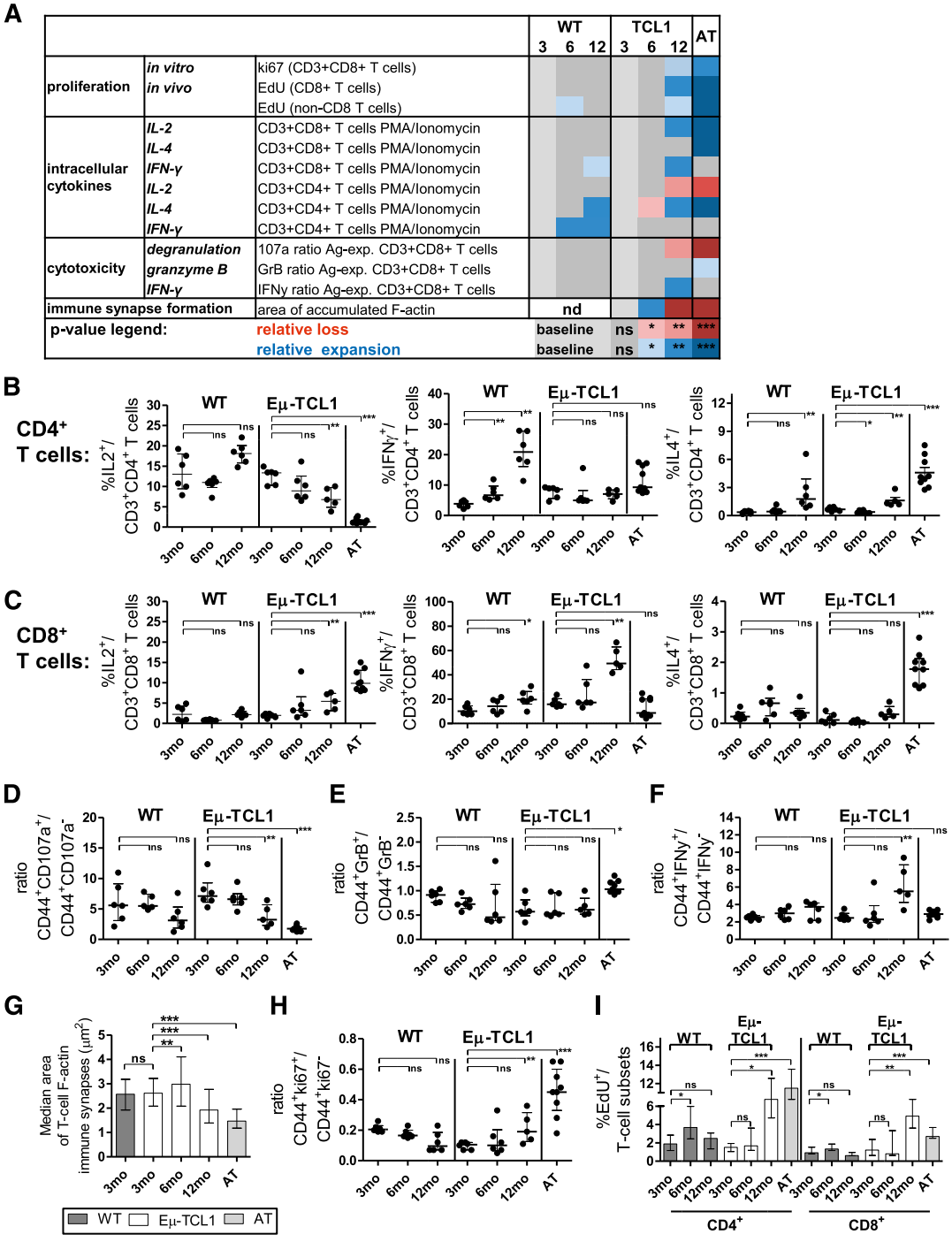

Figure 2. Longitudinal changes of T-cell functions in spleen as a representative organ in aging Eμ-TCL1 and WT mice and after AT. Fresh splenocytes from 3-, 6-, and 12-month-old WT and Eμ-TCL1 mice and from mice with full CLL after AT were stimulated for 6 hours with phorbol 12-myristate 13-acetate/ionomycin ± CD107a antibody in the presence of brefeldin/monensin for the last 5 hours of culture. Cells were then harvested, surface stained, fixed, permeabilized, and stained with antibodies against IL-2, IL-4, IFN-γ, and GrB. Unstimulated cells were used as controls and also stained with anti-ki-67 to assess proliferation. (A) Heat map summary of *P* values describing statistical differences in functional T-cell subsets. Groups were compared with the relative percentage of functional subsets in 3-month-old mice. Mann-Whitney test was used for nonnormally distributed data and unpaired *t* test for normally distributed data, as determined by Shapiro-Wilk normality test. Blue, relative expansion; red, relative loss of cell subsets; nd, no data; ns, nonsignificant. $^{*}P < .05$, $^{**}P < .001$, $^{***}P < .0001$. Percentages of (B) $CD3^{+}CD4^{+}$ and (C) $CD3^{+}CD8^{+}$ viable cells positive for IL-2, IL-4, and IFN-γ after mitogenic stimulation. Cells were gated based on unstimulated cell populations (supplemental Figure 1C). (D) Effector cell cytotoxicity was assessed by CD107a localization to the cell surface upon mitogenic stimulation. Naive/Ag-experienced viable $CD3^{+}CD8^{+}$ cytotoxic effector T-cell subsets were discriminated by expression of CD44. Unstimulated cells were used as controls. T-cell function was compared by calculating ratios of $CD44^{+}CD107a^{+}$ vs $CD44^{+}CD107a^{-}$ cells out of all $CD3^{+}CD8^{+}$ T cells to describe enrichment (increased ratio) or loss (decreased ratio) of effector cells within the $CD44^{+}$ population (supplemental Figure 1D). Longitudinal changes of intracellular (E) GrB and (F) IFN-γ were described in a similar fashion. (G) To assess changes in the ability to form immune synapse, splenic T cells were mixed with 7-amino-4-chloromethylcoumarin–labeled, super Ag-pulsed healthy B cells at a 1:1 ratio, centrifuged onto polylysine-coated microscope slides, and F-actin was stained with rhodamine-phalloidin. Synapse formation between T and B cells was quantified by confocal laser-scanning microscopy using AxioVision image analysis software. The synapse area is depicted as median area of T-cell F-actin immune synapses (μm^2) value. (H) Ex vivo proliferation of unstimulated $CD3^{+}CD8^{+}$ T cells was assessed by intranuclear ki-67 based on FMO controls and is given as a ratio among $CD44^{+}$ cells as described in panel D. (I) In vivo proliferation of $CD8^{+}$ and $CD4^{+}$ T cells was assessed after injection with 100 μg/g body weight EdU 20 hours before euthanasia as percentage of EdU^{+} cells after gating on $CD5^{+}$ $CD19^{-}$ cells (ie, T cells). All graphs depict median ± interquartile range and combine data from all cohorts of mice at each age group.

aged-matched WT and AT mice were stained for CD19/CD5. Increasing numbers of $CD19^+CD5^+$ CLL cells were detected in spleen, PB, and BM, but not yet in LNs, from 6-month-old Eμ-TCL1 mice, whereas 3-month-old Eμ-TCL1 and all WT mice were CLL-free (supplemental Figure 2A-C). AT of CLL cells into young mice consistently led to CLL development (meeting previously defined criteria) after a median of 7 weeks (range 3.71-20), with a very homogeneous disease load among individual mice. CLL development was significantly correlated (all P value Spearman correlation $\leq .0005$) with reduction in percentages of $CD3^+$ and $CD3^+CD4^+$ and expansion of $CD3^+CD8^+$ cells in spleen (Figure 1A), leading to the decrease of $CD4^+/CD8^+$ ratios (Figure 1B). This was recapitulated in PB, LNs, and (although not significantly) in BM (Figure 1C). Within $CD3^+CD8^+$ cells, $CD44^-CD62L^+$ naive cells were lost with CLL development and the population shifted toward $CD44^+$ antigen (Ag)-experienced cells in spleen (Figure 1D) and all examined organs (Figure 1F-H). In PB and LNs from aging Eμ-TCL1 mice, $CD44^+CD62L^+$ memory cells were significantly more frequent than $CD44^+CD62L^-$ effector cells (both $P < .0001$), whereas effector cells were more frequent (although not significant) in spleen ($P = .1884$) and BM ($P = .0682$; supplemental Tables 1 and 2). The spleen memory pool was further characterized by a shift toward $CCR7^-CD62L^-$ effector memory (EM) and a loss of $CCR7^+CD62L^+$ central memory cells (Figure 1E). Changes in AT mice were generally similar and showed less variance (Figure 1A-H; supplemental Table 1) and therefore demonstrated the suitability of this strategy to mirror phenotypic T-cell changes of aging CLL. However, exceptions were noted for LNs and BM $CD4^+/CD8^+$ ratios (Figure 1C) and EM differentiation (supplemental Tables 1 and 2). Some similarities in T-cell subset changes were also noted in aging WT mice (Figure 1A-H; supplemental Table 1). ANs of virtually all cell subsets increased in aging Eμ-TCL1 and after AT, but were largely stable in aging WT mice (supplemental Figure 3A). ANs of cells in other organs followed similar patterns (supplemental Figure 3B-D). Altogether, both longitudinal and direct comparison of aging Eμ-TCL1, WT, and AT mice led to characterization of CLL- and aging-specific T-cell phenotypes and highlighted differences between CLL-affected compartments and aging Eμ-TCL1 and AT mice (visualized in Figure 1I).

Developing CLL leads to characteristic functional changes in T-cell intracellular cytokines and effector function

We next investigated functional T-cell changes using splenocytes from 3-, 6-, and 12-month-old Eμ-TCL1, WT, and AT mice. Typical functional T-cell changes are summarized in Figure 2A. The development of CLL led to a loss of mitogen-stimulated $IL\text{-}2^+CD4^+$ cells and an impaired ability to increase the percentages of $IFN\text{-}\gamma^+CD4^+$ cells (Figure 2B). This was even more pronounced in AT mice. Among $CD8^+$ cells, the percentages of $IL\text{-}2^+CD8^+$ cells increased in aging Eμ-TCL1 and AT mice, whereas $IFN\text{-}\gamma^+CD8^+$ cells increased significantly in aging Eμ-TCL1 (Figure 2C). There were no differences in percentages of $IL\text{-}4^+CD4^+$ and $IL\text{-}4^+CD8^+$ cells between aging Eμ-TCL1 and WT mice (Figure 2B-C, right). AT mice were highly enriched for $IL\text{-}4^+CD4^+$ and $IL\text{-}4^+CD8^+$ cells, while lacking a significant increase in $IFN\text{-}\gamma^+CD4^+$ and $IFN\text{-}\gamma^+CD8^+$ cells, indicating a Th-2 skew probably from synchronized antigenic stimulation by the large disease burden.

Among Ag-experienced $CD44^+CD8^+$ cells, the $CD107a^+$:$CD107a^-$ ratio decreased in aging Eμ-TCL1 mice, signifying reduced percentages of cytotoxic cells, whereas aging WT mice only exhibited a nonsignificant trend (Figure 2D). GrB ratios decreased nonsignificantly in WT mice but were stable in aging Eμ-TCL1 mice (Figure 2E). Developing CLL in aging Eμ-TCL1 mice led to increased IFN-γ ratios that were not significant in AT mice (Figure 2F). Immune synapse formation was significantly impaired in 12-month-old Eμ-TCL1 and in AT mice, but not yet in 6-month-old TCL1 mice (Figure 2G). Of note, T-cell proliferation was increased with developing CLL and after AT, as evidenced by increased ki-67 ratios among $CD8^+CD44^+$ cells (Figure 2H); this was confirmed by in vivo EdU incorporation in $CD8^+$ and $CD4^+$ cells (Figure 2I). Because CD4 proliferation was increased, but the $CD4^+/CD8^+$ ratio fell, there must be increased CD4 cell death, although cell-survival studies were not performed.

High PD-L1/PD-L2 expression develop in the context of advancing disease and PD-L1 shows tissue-specific distribution

Because PD-L1/PD-1 are important mediators of T-cell dysfunction in human CLL, we next assessed PD-L1 expression on spleen CLL cells from fully leukemic Eμ-TCL1 (n = 8; median age 47 weeks; range 39.4-57.1) and AT mice (n = 12), and on $CD19^+$ B cells from age-matched WT mice (n = 12 total). Although the percentages of $PD\text{-}L1^+$ CLL/B cells were higher in leukemic than in WT mice (Figure 3A), but high in both groups, we observed more pronounced changes in corrected median fluorescence intensities (MFIs) (Figure 3B) and ANs (Figure 3C). Increased PD-L1 developed alongside advancing CLL, and could also be detected on CLL cells from other organs (Figure 3D, left). However, in 12-month-old Eμ-TCL1 mice, PD-L1 expression was higher in spleen (corrected MFI 4037 ± 428.3 standard deviation), LNs (2632 ± 736.5), and BM (2549 ± 864) than in PB (1886 ± 425.5), suggesting tissue-specific expression. A similar pattern was detected for PD-L2 expression (Figure 3D, right), but organ-specific expression was less apparent. This was again recapitulated in AT mice.

Aberrant PD-1 expression on $CD3^+CD8^+$ T cells develops as a result of CLL but is confounded by aging

With developing CLL, $CD3^+CD8^+$ cells upregulated expression of PD-1, the binding partner of PD-L1/PD-L2, which was also observed in aging WT mice (Figure 3F-G; supplemental Figure 4A, $\%PD1^+CD44^+CD3^+CD8^+$ cells at 12 months P value = .7513). This confounding effect of aging could be unmasked using AT into young recipients. ANs of $CD3^+CD8^+PD\text{-}1^+$ cells were significantly higher in Eμ-TCL1 and AT mice than in matched WT mice (Figure 3H). PD-1 induction by AT was confirmed by another experiment, in which recipient mice were randomized to AT with CLL or normal B cells (n = 9 each). This led to significantly higher expression of PD-1 in CLL-cell vs healthy B-cell recipients (supplemental Figure 4B), both on $CD44^+$ (supplemental Figure 4C) and on $CD44^-CD3^+CD8^+$ cells (supplemental Figure 4D). Similar patterns were observed for other inhibitory T-cell receptors including KLRG-1, 2B4, and LAG-3 (supplemental Figure 5A-D).

$PD\text{-}1^+$ normal T cells have markedly different effector functions than $PD\text{-}1^+$ CLL T cells

To investigate differences in T-cell function between $CD3^+CD8^+CD44^+PD\text{-}1^+$ T cells from those aging Eμ-TCL1 and WT mice, we also investigated ratios for CD107a, intracellular GrB/IFN-γ, and EdU in $PD\text{-}1^{high}$ and $PD\text{-}1^{low}$ spleen cells. In aging WT mice, CD107a ratios were comparable between $PD\text{-}1^{high}$ and $PD\text{-}1^{low}$ cells, indicating both subsets contain comparable proportions of cytotoxic cells (Figure 4A, left). With the onset of CLL at 6 months in Eμ-TCL1 mice, CD107a ratios were also similar in PD-1 subsets ($P = .5887$), but 2-fold higher

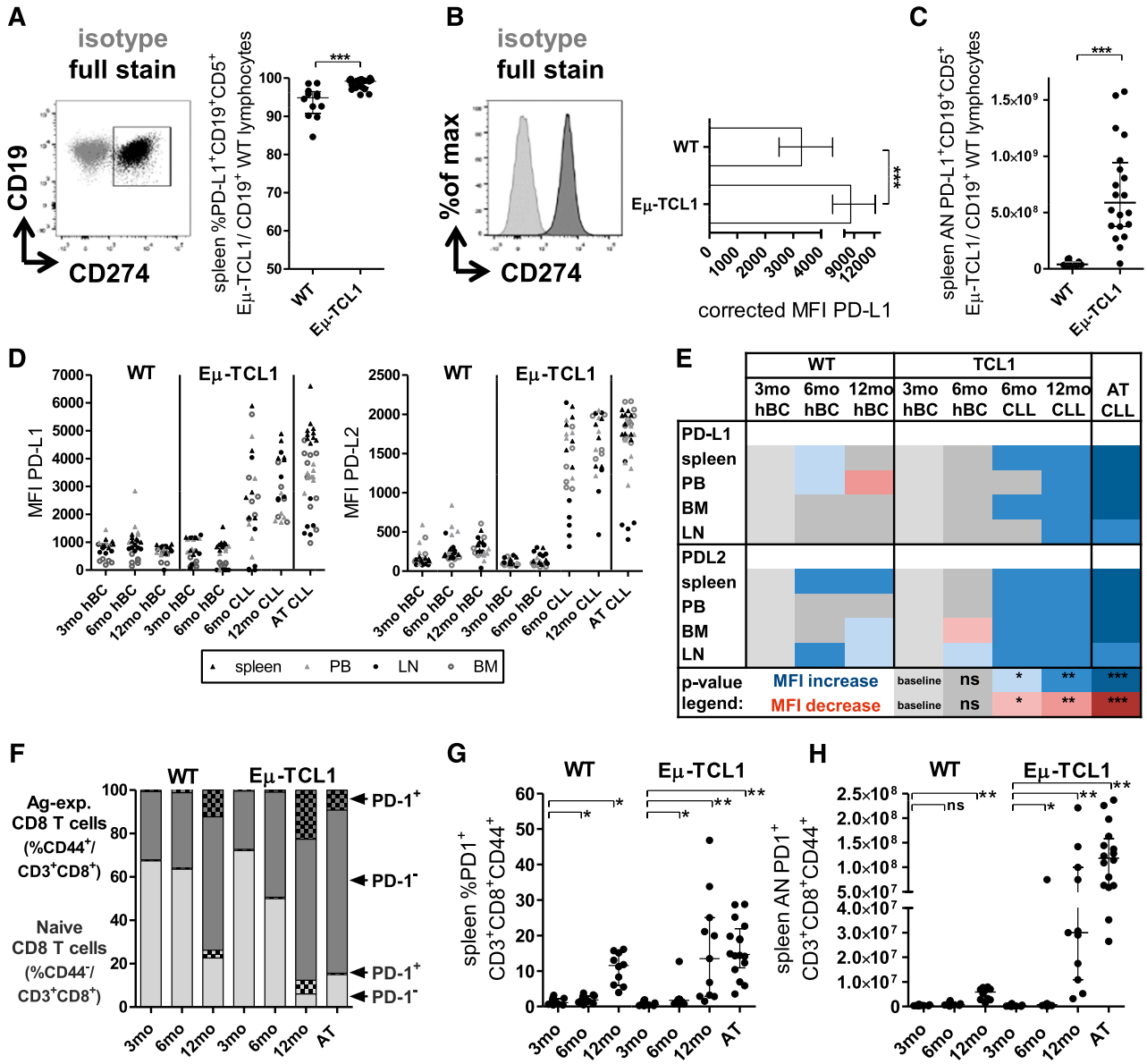

Figure 3. Longitudinal development of expression of PD-L1 and PD-L2 on CLL/normal B cells and PD-1 on CD3$^+$CD8$^+$ T cells. (A) Spleen cells from fully leukemic aged Eμ-TCL1 and AT mice meeting predefined end point criteria for CLL and age-matched WT mice were stained for CD19, CD5, and PD-L1; PD-L1 expression was compared between viable CD19$^+$CD5$^+$ CLL and CD19$^+$ B cells (a representative overlaid flow plot is depicted on the left, cells were gated based on FMO and isotype controls). (B) Representative histogram and differences of MFI corrected for the MFI of the FMO/isotype control of PD-L1 between fully leukemic Eμ-TCL1 and age-matched WT mice. (C) ANs were determined by normalizing percentages of cells to overall cell counts for spleen. (D) Longitudinal development of PD-L1 and PD-L2 expression across organs on healthy B cells (hBC) from 3-, 6-, 12-month-old WT and 3- and 6-month-old Eμ-TCL1 mice and on CLL cells from 6- and 12-month-old Eμ-TCL1 and AT mice (in 6-month-old Eμ-TCL1 mice, both CD19$^+$ normal and CD19$^+$CD5$^+$ malignant B cells exist next to each other and PD-L1/PD-L2 was gated on either population). (E) Heat map summary of *P* values describing statistical differences in MFI of PD-L1 and PD-L2 across organs. Groups were compared with corrected MFIs in 3-month-old mice. Blue, increase; red, decrease of MFI; ns, nonsignificant. *$P < .05$, **$P < .001$, ***$P < .0001$. (F) At least 2 cohorts of 3-, 6-, and 12-month-old Eμ-TCL1, WT, and AT mice containing ≥5 mice each were euthanized; splenocytes were stained for CD3, 4, 8, 62L, 44, and PD-1 and assessed in relation to CLL load (supplemental Figure 1). Quantification of PD-1 expression in the context of T-cell CD3$^+$CD8$^+$CD44$^+$ subset changes. Stacked bar charts are used to visualize the loss of naive (light gray) and shift to Ag-experienced cells (dark gray). Longitudinal changes of (G) percentages and (H) ANs of PD-1$^+$CD3$^+$CD8$^+$CD44$^+$ cells. All graphs depict median ± interquartile range, and combine data from at all cohorts of mice at each age group.

than in age-matched WT mice, suggesting enrichment for cytotoxic T cells (Figure 4A, right). With progressive CLL, both subsets lost cytotoxic cells, leading to a significant decrease in ratios, with ratios lower in PD-1^{high} than in PD-1^{low} cells ($P = .0222$).

Effector ratios for GrB were 2-3 times higher in PD-1^{high} than in PD-1^{low} cells in aging WT mice (6 months: $P = .0087$; 12 months: $P = .0931$), suggesting that PD-1^{high} cells are enriched for GrB$^+$ cells (Figure 4B, left). In aging Eμ-TCL1 mice, there was no longer a difference in GrB expression in PD-1^{high} compared with PD-1^{low} cells (6 months: $P = .8726$; 12 months: $P = .2948$; Figure 4B, right). Similarly, IFN-γ ratios were higher in PD-1^{high} than in PD-1^{low} cells (6 months: $P = .026$; 12 months: $P = .0043$) in aging WT mice. In 6-month-old Eμ-TCL1 mice, PD-1 subset ratios were not different from each other ($P = .3095$, Figure 4C, right). Moreover, the significantly increased IFN-γ production associated with advanced CLL could be attributed to both PD-1 subsets ($P = 1.0$, Figure 4C, left).

EdU ratios were comparable between PD-1^{high} and PD-1^{low} cells in aging WT mice (Figure 4D, left). CLL-induced increased T-cell

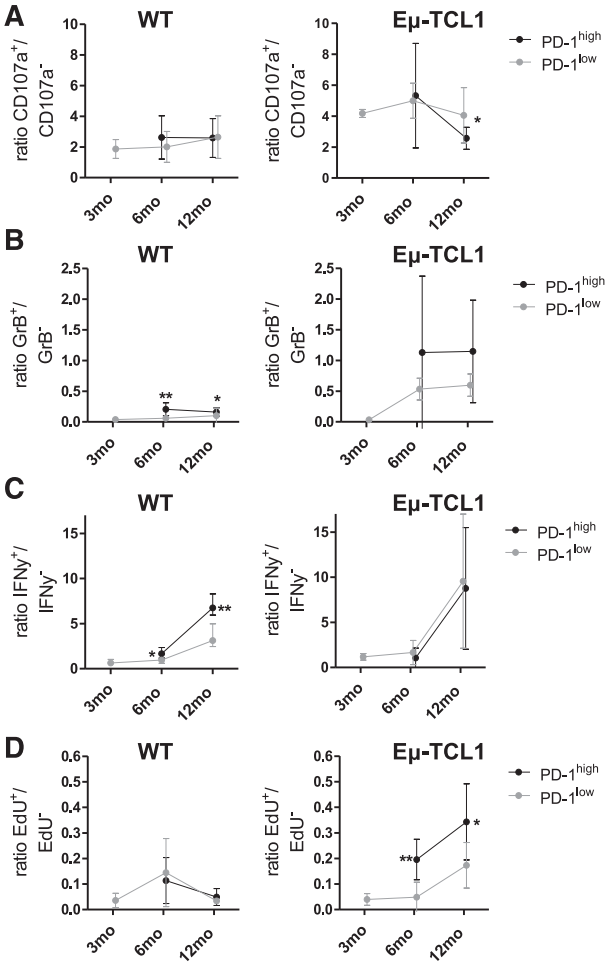

Figure 4. Associations between PD-1 expression and effector functions in T cells from aging healthy WT mice and Eμ-TCL1 mice. Fresh splenocytes from 3-, 6, and 12-month-old WT and Eμ-TCL1 mice were processed and stained as described in Figure 2. Ratios for (A) CD107a degranulation, (B) intracellular GrB, (C) IFN-γ, and (D) EdU proliferation were compared between PD-1^{high} and PD-1^{low} CD3$^+$CD8$^+$CD44$^+$ cells in WT and Eμ-TCL1 mice. Three-month-old mice had no detectable PD-1 expression; effector function was therefore determined on PD-1^{low} cells only. All graphs show median with interquartile range. ns, nonsignificant, $^*P < .05$, $^{**}P < .001$, $^{***}P < .0001$.

proliferation was attributed to both PD-1 subsets, with the PD-1^{high} ratio being significantly higher than the PD-1^{low} ratio (6 months: $P = .0087$; 12 months: $P = .0317$; Figure 4D, right), suggesting that increased T-cell proliferation is predominantly accounted for by PD-1^{high} cells.

The effect of PD-1 expression on immune synapse was further examined in AT mice. Compared with normal CD8$^+$ T cells, the ability of CLL CD8$^+$ T cells to form synapses with healthy B cells as Ag-presenting cells was significantly impaired ($P < .0001$). However, PD-1^{low}CD8$^+$ T cells formed larger synapses than PD-1^{high}CD8$^+$ T cells ($P < .0001$), indicating that the impaired ability of CD8$^+$ T cells seems to be promoted by the PD-1^{high} subset (Figure 5A-B).

Discussion

We used the Eμ-TCL1 mouse model and aged-matched WT mice as a preclinical platform to examine patterns of T-cell dysfunction in the context of developing CLL in different microenvironments and in direct comparison with aging-related T-cell defects, with a focus on PD-1/PD-L1/PD-L2, which are a major immunosuppressive mechanism in CLL.[4,7,18] Previous studies in Eμ-TCL1 mice demonstrated that molecular T-cell defects and subset changes can be modeled in leukemic mice,[28,29,32] but have failed to take full advantage of the availability of different microenvironments. In CLL patients, T-cell defects and associations with aggressive disease/poor outcome have been extensively characterized,[3,4,6,18,33-37] but have focused largely on PB. However, different organs provide distinct and unique microenvironments for CLL cells,[20,21] and it is not known if the same holds true for T cells. Moreover, fundamental T-cell defects are also present in aging healthy individuals,[38] which needs to be taken into account because CLL is predominantly a disease of the elderly. AT of CLL into young mice allows elimination of the confounding variable of aging and is a widely accepted strategy to shorten disease latency[39] and decrease variability. To understand the full potential of this approach, especially in the context of immunotherapy, and its suitability to mirror T-cell dysfunction in aging Eμ-TCL1 mice, AT requires thorough characterization.

We first examined T-cell phenotype as a surrogate marker for T-cell defects with similarities between humans[4,33-37] and mice[29] with CLL in different organs, with a focus on CD3$^+$CD8$^+$ cells. We demonstrate that developing CLL leads to T-cell subset changes across all organs, but that these are partly mirrored in aging leukemia-free mice, confirming aging as an important confounder. The direct comparison between aged leukemic Eμ-TCL1 and WT mice confirmed that the CLL-induced reduction of CD4/CD8 ratios and the shift between naive/Ag-experienced cells is observed across CLL-affected compartments. However, specific organs influenced effector/memory subset differentiation, suggesting the microenvironment might skew determination of T-cell effector/memory fate,[40] with immune-cell subsets reciprocally providing pro-survival stimuli to CLL cells.[41] Although the underlying mechanisms remain under investigation, our data deliver valuable first evidence that organs affect T-cell properties, which will inform future studies on immune-evasion mechanisms. The AT model was very reproducible and, while recapitulating changes in aging Eμ-TCL1 mice, was more skewed toward EM cells. This is very similar to our observations in human patients[4] and might reflect the increased aggressiveness of this approach resulting from synchronized onset of antigenic stimulation and large disease burden. Exceptions were also noted for LNs. We injected higher CLL doses than others,[29] which shortened disease latency but might have favored homing of CLL cells to other organs. As a result, induction of LN involvement by AT did not fully mirror LN involvement in aging mice.

The development of CLL also led to characteristic changes in T-cell cytokines and effector function, which were distinct from aging WT mice. This was even more pronounced after AT, most likely because of the increased immunosuppressive effect exerted by synchronized onset of antigenic stimulation. Interestingly, in aging Eμ-TCL1 mice, significant functional changes were not apparent until later stages of CLL. Immune synapse formation was actually improved in 6-month-old Eμ-TCL1 mice, indicating that cytotoxic functions might be maintained as a result of compensation by "overfunctioning" immune synapses in early stages of Ag encounter with CLL. Surprisingly, CD8$^+$ T-cell proliferation increased with developing CLL and after AT, in contrast to our human work, which found a proliferative defect in PB CLL T cells.[4] These discrepancies can potentially be attributed to a compartment-specific effect, as described for CLL cells,[41] or by different dynamics in humans in which patients may have had the disease for a long period before they are diagnosed and studied. Further studies will be needed to address the effect of the microenvironment on T-cell proliferation

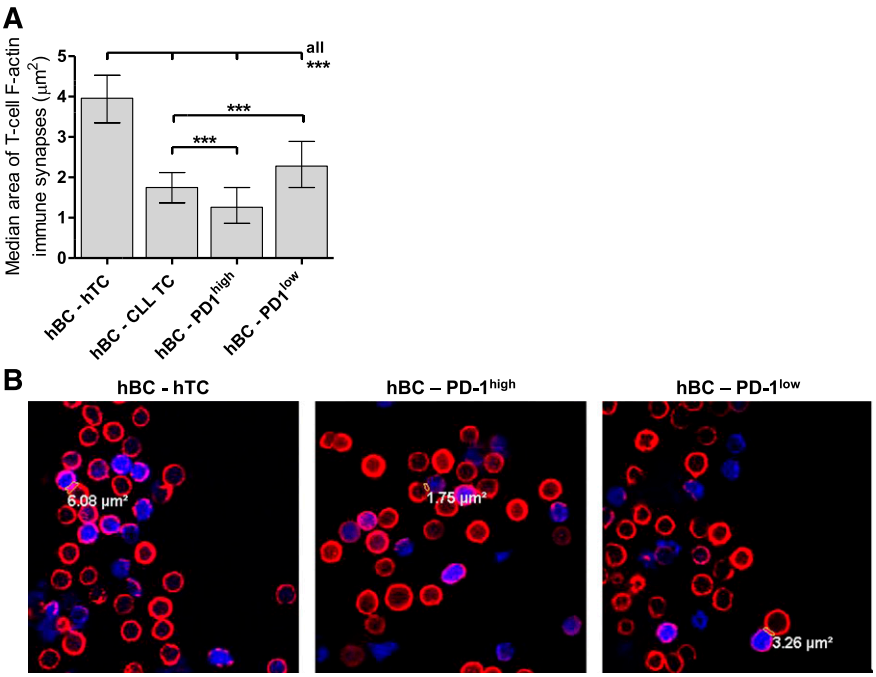

Figure 5. Immune synapse formation between B and T cells according to PD-1 expression. Spleen cells from mice with CLL after AT (n = 5) and age-matched WT mice (n = 3) were debulked of CLL/B cells using magnetic beads; stained for CD3, 8, and PD-1; and flow-sorted into $CD3^+CD8^+$, $CD3^+CD8^+$ $PD\text{-}1^{high}$, and $CD3^+CD8^+PD\text{-}1^{low}$ cells. Cells from WT mice were sorted on $CD3^+CD8^+$ only. (A) Comparison of median areas of immune synapses (μm^2) between normal B and $CD8^+$ T cells (hBC-hTC), normal B cells and CLL T cells (hBC-CLL TC), normal B cells and $PD\text{-}1^{low}CD8^+$ T cells (hBC-$PD\text{-}1^{low}$), and normal B cells and $PD\text{-}1^{high}CD8^+$ T cells (hBC-$PD\text{-}1^{high}$). ns, non-significant. $^*P < .05$, $^{**}P < .001$, $^{***}P < .0001$. (B) Representative confocal images of synapses taken with a ×63 objective between hBC-hTC, hBC- $PD\text{-}1^{high}$, and hBC-$PD\text{-}1^{low}$ cells. Blue, amino-4-chloromethylcoumarin–labeled B cells; red, rhodamine phalloidin staining actin cytoskeleton.

in vivo and include subsets of $CD4^+$ T cells to further understand their importance for CLL cell migration, survival, and proliferation.[22,42,43]

Inhibition of the PD-1/PD-L1 axis is emerging as a very attractive therapeutic target in cancer.[44-46] To understand fully the potential of such approaches in CLL, we characterized mechanisms of PD-1/PD-L1–mediated T-cell dysfunction in the Eμ-TCL1 model. We found that highly increased PD-L1—as in human CLL[7] is characteristic of murine CLL cells—can be detected in all organs, but is highest in spleen, suggesting a modulating effect of the microenvironment. This is an important finding because tissue-specific differences selectively support the persistence of PD-L1–mediated defects in infection models[47] and might explain the tumor-protecting effects of microenvironmental niches. Similar patterns but less tissue specificity were found for PD-L2, verifying its relevance as another inhibitory molecule in CLL.[48,49] In solid malignancies, PD-L1 appears to be the dominant negative molecule, with PD-L2 expressed in only a minority of patients.[50-52]

As found in human cancers, $CD3^+CD8^+$ T cells from leukemic mice expressed PD-1, with other inhibitory ligands including KLRG-1, 2B4, and LAG-3, highlighting potential synergisms between coinhibitory receptors described in other murine cancer models.[32,53] Although aging healthy mice also showed increased PD-1 expression, we detected marked differences on the functional impact of PD-1 expression. Contrasting with the notion that increased PD-1 expression would directly impact T-cell function in CLL, we found maintained cytotoxicity in $PD\text{-}1^{high}$ T cells, but their ability to form immune synapses was significantly impaired compared with $PD\text{-}1^{low}$ cells, potentially from a direct effect on forming microclusters[54] or an inhibition of Lck/integrin signaling.[3,55] However, compared with age-matched WT mice, defects in IFN-γ and GrB expression became apparent in $PD\text{-}1^{high}$ compared with $PD\text{-}1^{low}$ T cells from ageing Eμ-TCL1 mice. However, this did not render them nonfunctional. Interestingly, CLL-induced increased T-cell proliferation was mainly driven by $PD\text{-}1^{high}$ cells. Altogether, these findings indicate that despite similar PD-1 expression patterns, $PD\text{-}1^+$ T cells in the absence of CLL have markedly different effector functions than $PD\text{-}1^+$ T cells in the presence of disease. Moreover, they identify $PD\text{-}1^+$ T cells in CLL as a functionally heterogeneous population in which key immunological nodes (ie, recognition, generation of effector cells, effector potential) are affected in different ways. The paradigm that there is global inhibition of T-cell function in CLL has been previously challenged by the observation that cytomegalovirus-specific $CD8^+$ T cells were functionally intact, whereas CLL-induced global T-cell defects were still present.[56] Our findings add to this theory and suggest that global PD-1 expression is not a definite marker of T-cell dysfunction, but that the functional inhibition of T cells by CLL might also be determined by antigenic identity, the differentiation state of T cells, and/or the microenvironmental compartment. This indicates that interactions of CLL cells with the adaptive immune system may be quite specific, with tumor cells suppressing certain subpopulations of T cells. Parallel to exhaustion models, in which exhausted $CD8^+$ T cells continued their differentiation process upon transfer into healthy mice,[16] and function could be rescued in specific $PD\text{-}1^+$ populations by antibody blockade,[17] similar therapeutic approaches might be attractive in CLL. Although the contribution of other humoral and cellular immune regulators (eg, $CD4^+$ subsets, regulatory T cells, natural killer/myeloid cells) within different microenvironments still needs to be established, this study has provided insight into compartment-specific mechanisms of PD-L1/PD-1–mediated $CD8^+$ T-cell dysfunction in the context of aging-related immune defects. Our findings indicate that reinvigorated antitumor immune function might be achieved by both reprogramming and selective expansion of T-cell subsets, but that specific tumor microenvironments might continue to provide tumor-protective niches, favoring therapeutic blockade of PD-L1.

Acknowledgments

This work was supported by grants from Deutsche Krebshilfe (F.M.) by the Helmholtz Virtual Institute (J.G.G., F.M.), and from the National Institutes of Health, National Cancer Institute for the CLL Research Consortium (grant P01 CA95426) (J.G.G., D.N., C.M.C.).

Authorship

Contribution: F.M. designed, performed, and analyzed the experiments; collected the samples, and wrote the manuscript; J.C.R. designed and analyzed experiments; S.M. cared for animals, collected samples, and performed experiments; W.P.D. and E.K. performed, analyzed, and interpreted experiments; D.N. designed and analyzed experiments and data and provided statistical support; C.M.C. provided Eμ-TCL1 breeding pairs, interpreted data, and edited the manuscript; M.C. designed and analyzed experiments and edited the manuscript; and J.G.G. designed the experiments and interpreted the data, wrote and edited the manuscript, and supervised the study.

Conflict-of-interest disclosure: The authors declare no competing financial interests.

Correspondence: John G. Gribben, Barts Cancer Institute, Queen Mary University of London, 3rd Floor John Vane Science Centre, Charterhouse Square, London, EC1M 6BQ, United Kingdom; e-mail: j.gribben@qmul.ac.uk.

References

1. Burger JA, Gribben JG. The microenvironment in chronic lymphocytic leukemia (CLL) and other B cell malignancies: insight into disease biology and new targeted therapies. *Semin Cancer Biol.* 2014;24:71-81.
2. Riches JC, Gribben JG. Understanding the immunodeficiency in chronic lymphocytic leukemia: potential clinical implications. *Hematol Oncol Clin North Am.* 2013;27(2):207-235.
3. Ramsay AG, Johnson AJ, Lee AM, et al. Chronic lymphocytic leukemia T cells show impaired immunological synapse formation that can be reversed with an immunomodulating drug. *J Clin Invest.* 2008;118(7):2427-2437.
4. Riches JC, Davies JK, McClanahan F, et al. T cells from CLL patients exhibit features of T-cell exhaustion but retain capacity for cytokine production. *Blood.* 2013;121(9):1612-1621.
5. Ramsay AG, Evans R, Kiaii S, Svensson L, Hogg N, Gribben JG. Chronic lymphocytic leukemia cells induce defective LFA-1-directed T-cell motility by altering Rho GTPase signaling that is reversible with lenalidomide. *Blood.* 2013;121(14): 2704-2714.
6. Görgün G, Holderried TAW, Zahrieh D, Neuberg D, Gribben JG. Chronic lymphocytic leukemia cells induce changes in gene expression of CD4 and CD8 T cells. *J Clin Invest.* 2005;115(7): 1797-1805.
7. Ramsay AG, Clear AJ, Fatah R, Gribben JG. Multiple inhibitory ligands induce impaired T-cell immunologic synapse function in chronic lymphocytic leukemia that can be blocked with lenalidomide: establishing a reversible immune evasion mechanism in human cancer. *Blood.* 2012;120(7):1412-1421.
8. Day CL, Kaufmann DE, Kiepiela P, et al. PD-1 expression on HIV-specific T cells is associated with T-cell exhaustion and disease progression. *Nature.* 2006;443(7109):350-354.
9. Petrovas C, Casazza JP, Brenchley JM, et al. PD-1 is a regulator of virus-specific CD8+ T cell survival in HIV infection. *J Exp Med.* 2006; 203(10):2281-2292.
10. Wherry EJ. T cell exhaustion. *Nat Immunol.* 2011; 12(6):492-499.
11. Blackburn SD, Shin H, Haining WN, et al. Coregulation of CD8+ T cell exhaustion by multiple inhibitory receptors during chronic viral infection. *Nat Immunol.* 2009;10(1):29-37.
12. Freeman GJ, Long AJ, Iwai Y, et al. Engagement of the PD-1 immunoinhibitory receptor by a novel B7 family member leads to negative regulation of lymphocyte activation. *J Exp Med.* 2000;192(7): 1027-1034.
13. Latchman Y, Wood CR, Chernova T, et al. PD-L2 is a second ligand for PD-1 and inhibits T cell activation. *Nat Immunol.* 2001;2(3):261-268.
14. Nishimura H, Nose M, Hiai H, Minato N, Honjo T. Development of lupus-like autoimmune diseases by disruption of the PD-1 gene encoding an ITIM motif-carrying immunoreceptor. *Immunity.* 1999; 11(2):141-151.
15. Zinselmeyer BH, Heydari S, Sacristán C, et al. PD-1 promotes immune exhaustion by inducing antiviral T cell motility paralysis. *J Exp Med.* 2013; 210(4):757-774.
16. Utzschneider DT, Legat A, Fuertes Marraco SA, et al. T cells maintain an exhausted phenotype after antigen withdrawal and population reexpansion. *Nat Immunol.* 2013;14(6):603-610.
17. Blackburn SD, Shin H, Freeman GJ, Wherry EJ. Selective expansion of a subset of exhausted CD8 T cells by alphaPD-L1 blockade. *Proc Natl Acad Sci USA.* 2008;105(39):15016-15021.
18. Brusa D, Serra S, Coscia M, et al. The PD-1/PD-L1 axis contributes to T-cell dysfunction in chronic lymphocytic leukemia. *Haematologica.* 2013; 98(6):953-963.
19. Duraiswamy J, Ibegbu CC, Masopust D, et al. Phenotype, function, and gene expression profiles of programmed death-1(hi) CD8 T cells in healthy human adults. *J Immunol.* 2011;186(7): 4200-4212.
20. Mittal AK, Chaturvedi NK, Rai KJ, et al. Chronic lymphocytic leukemia cells in a lymph node microenvironment depict molecular signature associated with an aggressive disease. *Mol Med.* 2014;20(1):290-301.
21. Herishanu Y, Pérez-Galán P, Liu D, et al. The lymph node microenvironment promotes B-cell receptor signaling, NF-kappaB activation, and tumor proliferation in chronic lymphocytic leukemia. *Blood.* 2011;117(2):563-574.
22. Ghia P, Granziero L, Chilosi M, Caligaris-Cappio F. Chronic B cell malignancies and bone marrow microenvironment. *Semin Cancer Biol.* 2002; 12(2):149-155.
23. Patten PEM, Buggins AGS, Richards J, et al. CD38 expression in chronic lymphocytic leukemia is regulated by the tumor microenvironment. *Blood.* 2008;111(10):5173-5181.
24. Quijano S, López A, Rasillo A, et al. Association between the proliferative rate of neoplastic B cells, their maturation stage, and underlying cytogenetic abnormalities in B-cell chronic lymphoproliferative disorders: analysis of a series of 432 patients. *Blood.* 2008;111(10):5130-5141.
25. Smit LA, Hallaert DY, Spijker R, et al. Differential Noxa/Mcl-1 balance in peripheral versus lymph node chronic lymphocytic leukemia cells correlates with survival capacity. *Blood.* 2007; 109(4):1660-1668.
26. Davids MS, Deng J, Wiestner A, et al. Decreased mitochondrial apoptotic priming underlies stroma-mediated treatment resistance in chronic lymphocytic leukemia. *Blood.* 2012;120(17): 3501-3509.
27. Bichi R, Shinton SA, Martin ES, et al. Human chronic lymphocytic leukemia modeled in mouse by targeted TCL1 expression. *Proc Natl Acad Sci USA.* 2002;99(10):6955-6960.
28. Gorgun G, Ramsay AG, Holderried TAW, et al. E(mu)-TCL1 mice represent a model for immunotherapeutic reversal of chronic lymphocytic leukemia-induced T-cell dysfunction. *Proc Natl Acad Sci USA.* 2009;106(15): 6250-6255.
29. Hofbauer JP, Heyder C, Denk U, et al. Development of CLL in the TCL1 transgenic mouse model is associated with severe skewing of the T-cell compartment homologous to human CLL. *Leukemia.* 2011;25(9):1452-1458.
30. Saulep-Easton D, Vincent FB, Le Page M, et al. Cytokine-driven loss of plasmacytoid dendritic cell function in chronic lymphocytic leukemia. *Leukemia.* 2014;28(10):2005-2015.
31. Betts MR, Brenchley JM, Price DA, et al. Sensitive and viable identification of antigen-specific CD8+ T cells by a flow cytometric assay for degranulation. *J Immunol Methods.* 2003; 281(1-2):65-78.
32. Göthert JR, Eisele L, Klein-Hitpass L, et al. Expanded CD8+ T cells of murine and human CLL are driven into a senescent KLRG1+ effector memory phenotype. *Cancer Immunol Immunother.* 2013;62(11):1697-1709.
33. Catovsky D, Miliani E, Okos A, Galton DA. Clinical significance of T-cells in chronic lymphocytic leukaemia. *Lancet.* 1974;2(7883):751-752.
34. Herrmann F, Lochner A, Philippen H, Jauer B, Rühl H. Imbalance of T cell subpopulations in patients with chronic lymphocytic leukaemia of the B cell type. *Clin Exp Immunol.* 1982;49(1): 157-162.
35. Platsoucas CD, Galinski M, Kempin S, Reich L, Clarkson B, Good RA. Abnormal T lymphocyte subpopulations in patients with B cell chronic lymphocytic leukemia: an analysis by monoclonal antibodies. *J Immunol.* 1982;129(5):2305-2312.
36. Nunes C, Wong R, Mason M, Fegan C, Man S, Pepper C. Expansion of a CD8(+)PD-1(+) replicative senescence phenotype in early stage CLL patients is associated with inverted CD4:CD8 ratios and disease progression. *Clin Cancer Res.* 2012;18(3):678-687.
37. Rissiek A, Schulze C, Bacher U, et al. Multidimensional scaling analysis identifies pathological and prognostically relevant profiles of circulating T-cells in chronic lymphocytic leukemia. *Int J Cancer.* 2014;135(10):2370-2379.
38. Nikolich-Žugich J. Aging of the T cell compartment in mice and humans: from no naive expectations to foggy memories. *J Immunol.* 2014;193(6):2622-2629.
39. Simonetti G, Bertilaccio MTS, Ghia P, Klein U. Mouse models in the study of chronic lymphocytic leukemia pathogenesis and therapy. *Blood.* 2014; 124(7):1010-1019.
40. Chang JT, Wherry EJ, Goldrath AW. Molecular regulation of effector and memory T cell differentiation. *Nat Immunol.* 2014;15(12): 1104-1115.

41. Heinig K, Gätjen M, Grau M, et al. Access to follicular dendritic cells is a pivotal step in murine chronic lymphocytic leukemia B-cell activation and proliferation. *Cancer Discov.* 2014;4(12): 1448-1465.

42. Os A, Bürgler S, Ribes AP, et al. Chronic lymphocytic leukemia cells are activated and proliferate in response to specific T helper cells. *Cell Reports.* 2013;4(3):566-577.

43. Bagnara D, Kaufman MS, Calissano C, et al. A novel adoptive transfer model of chronic lymphocytic leukemia suggests a key role for T lymphocytes in the disease. *Blood.* 2011; 117(20):5463-5472.

44. Ansell SM, Lesokhin AM, Borrello I, et al. PD-1 blockade with nivolumab in relapsed or refractory Hodgkin's lymphoma. *N Engl J Med.* 2015;372(4): 311-319.

45. Brahmer JR, Tykodi SS, Chow LQM, et al. Safety and activity of anti-PD-L1 antibody in patients with advanced cancer. *N Engl J Med.* 2012;366(26): 2455-2465.

46. Topalian SL, Hodi FS, Brahmer JR, et al. Safety, activity, and immune correlates of anti-PD-1 antibody in cancer. *N Engl J Med.* 2012;366(26): 2443-2454.

47. Blackburn SD, Crawford A, Shin H, Polley A, Freeman GJ, Wherry EJ. Tissue-specific differences in PD-1 and PD-L1 expression during chronic viral infection: implications for CD8 T-cell exhaustion. *J Virol.* 2010;84(4):2078-2089.

48. Steidl C, Shah SP, Woolcock BW, et al. MHC class II transactivator CIITA is a recurrent gene fusion partner in lymphoid cancers. *Nature.* 2011; 471(7338):377-381.

49. Taube JM, Klein A, Brahmer JR, et al. Association of PD-1, PD-1 ligands, and other features of the tumor immune microenvironment with response to anti-PD-1 therapy. *Clin Cancer Res.* 2014;20(19): 5064-5074.

50. Ohigashi Y, Sho M, Yamada Y, et al. Clinical significance of programmed death-1 ligand-1 and programmed death-1 ligand-2 expression in human esophageal cancer. *Clin Cancer Res.* 2005;11(8):2947-2953.

51. Nomi T, Sho M, Akahori T, et al. Clinical significance and therapeutic potential of the programmed death-1 ligand/programmed death-1 pathway in human pancreatic cancer. *Clin Cancer Res.* 2007;13(7):2151-2157.

52. Hamanishi J, Mandai M, Iwasaki M, et al. Programmed cell death 1 ligand 1 and tumor-infiltrating CD8+ T lymphocytes are prognostic factors of human ovarian cancer. *Proc Natl Acad Sci USA.* 2007;104(9):3360-3365.

53. Woo SR, Turnis ME, Goldberg MV, et al. Immune inhibitory molecules LAG-3 and PD-1 synergistically regulate T-cell function to promote tumoral immune escape. *Cancer Res.* 2012;72(4): 917-927.

54. Yokosuka T, Takamatsu M, Kobayashi-Imanishi W, Hashimoto-Tane A, Azuma M, Saito T. Programmed cell death 1 forms negative costimulatory microclusters that directly inhibit T cell receptor signaling by recruiting phosphatase SHP2. *J Exp Med.* 2012;209(6): 1201-1217.

55. Morgan MM, Labno CM, Van Seventer GA, Denny MF, Straus DB, Burkhardt JK. Superantigen-induced T cell:B cell conjugation is mediated by LFA-1 and requires signaling through Lck, but not ZAP-70. *J Immunol.* 2001;167(10): 5708-5718.

56. te Raa GD, Pascutti MF, García-Vallejo JJ, et al. CMV-specific CD8+ T-cell function is not impaired in chronic lymphocytic leukemia. *Blood.* 2014;123(5):717-724.